

Stochastic Causal Programming for Bounding Treatment Effects

Kirtan Padh¹, Jakob Zeitler², David Watson², Matt Kusner², Ricardo Silva², Niki Kilbertus^{1,3}

¹Helmholtz AI, Munich

²University College London

³Technical University of Munich

Corresponding author: kirtan.padh@helmholtz-muenchen.de

Abstract

Causal effect estimation is important for numerous tasks in the natural and social sciences. However, identifying effects is impossible from observational data without making strong, often untestable assumptions. We consider algorithms for the *partial* identification problem, bounding treatment effects from multivariate, continuous treatments over multiple possible causal models when unmeasured confounding makes identification impossible. We consider a framework where observable evidence is matched to the implications of constraints encoded in a causal model by norm-based criteria. This generalizes classical approaches based purely on generative models. Casting causal effects as objective functions in a constrained optimization problem, we combine flexible learning algorithms with Monte Carlo methods to implement a family of solutions under the name of *stochastic causal programming*. In particular, we present ways by which such constrained optimization problems can be parameterized without likelihood functions for the causal or the observed data model, reducing the computational and statistical complexity of the task.

1 Introduction

Estimating causal effects is a key goal of scientific inquiry, enabling better decision making in medicine (Bica et al., 2021), economics (Chernozhukov et al., 2018), epidemiology (Vandenbroucke et al., 2016), and beyond (Pearl, 2009; Imbens and Rubin, 2015). The gold standard for estimating these effects is the randomized controlled trial (RCT): randomly assign individuals to treatment and control groups (e.g., vaccine or placebo) and observe outcomes (e.g., antibody levels). These experiments work because randomization removes *confounding*, which occurs when pre-treatment covariates drive both treatment propensities and potential outcomes. However, in many cases it is physically, logically, or ethically impossible to conduct RCTs. In such cases, causal effects can only be identified under structural assumptions (Shpitser and Pearl, 2008).

Well-studied approaches for inferring causal effects from observational data in the presence of unobserved confounding include the instrumental variable (IV) model and mediation analysis via front-door adjustment. In IV models, we estimate the causal effect of X on Y despite the presence of latent confounder U by use of an *instrument* Z , which only influences Y through X (see Figure 1a. for a graphical depiction and Section 2 for a formal definition). For example, Fisher (1957) famously argued that the observed association between smoking X and lung cancer Y could be due to some unobserved genotype U that serves as a common cause for both. We can test this hypothesis with access to an instrument—e.g., a tobacco tax Z , which exerts negative pressure on cigarette consumption but has no direct effect on lung cancer. In the front-door setting, a latent confounder U between X and Y can be dealt

with by assuming that the causal influence of X on Y is mediated by an observed variable M not directly affected by U : $X \rightarrow M \rightarrow Y$ (see Section 2 for a formal definition). Again, if we assume that lung cancer Y is only directly caused by tar deposits in the lungs M , which increase with smoking X , the causal effect can be identified.

Even in these cases, exact identification requires restrictive assumptions, not just about the graphical structure but about the functional form of causal associations, e.g., monotonicity (Angrist and Imbens, 1995) or additivity (Hartford et al., 2017; Singh et al., 2019; Muandet et al., 2020; Bennett et al., 2019). When such assumptions fail, effects may still be *partially identifiable*—i.e., bounded with respect to a set of models consistent with the data (Manski, 1990). This task has not received nearly as much attention as the point estimation problem, despite promising early work in this area (Chickering and Pearl, 1996; Balke and Pearl, 1997). Lately the topic has sparked some interest in reinforcement learning (Kallus and Zhou, 2020; Zhang and Bareinboim, 2020) and algorithmic fairness (Wu et al., 2019a,b), as well as other nonparametric prediction settings (Gunsilius, 2019; Zhang and Bareinboim, 2021; Hu et al., 2021). Xia et al. (2021) outline a general procedure for bounding causal effects with neural networks, but restrict their focus to discrete, low-dimensional data. In a recent paper, Kilbertus et al. (2020b) propose a method for computing causal bounds in IV models with continuous treatments using gradient descent and Monte Carlo integration. Unfortunately, because their procedure relies on discretizing the instrument Z and inverse CDF sampling for the treatment X , it is limited to univariate settings (see Appendix G for further limitations).

We extend this work to higher dimensions and different

causal structures, replacing the copula formulation of Kilbertus et al. (2020b) with a more generic parameterization that decouples model fitting from changes due to the unobserved confounder U . We take inspiration from classical sensitivity analysis (Saltelli, 2002), where the goal is to predict plausible outcomes given some fixed function class and set of perturbations. In this causal reformulation, we quantify the range of possible treatment effects for a family of models that agree on the marginal distribution of the observed data by spanning values for the unobserved potential outcomes (Franks et al., 2019). Grid search becomes exponentially difficult as dimensionality grows, so we replace the discretization approach with a stochastic, differentiable procedure for solving the constrained optimization problem. This parameterization is related to recent literature on (conditional) normalizing flows (Papamakarios et al., 2021), where base distributions are converted into targets through some diffeomorphic transformation(s). Whereas the goal in flow models is typically generative, the sampling step in our method is a means toward the end of causal effect bounding.

We make the following contributions: (1) We propose a generic, modular form of the treatment effect bounding problem that is compatible with a wide range of graphical structures, function classes, optimization procedures, and distance measures, as well as a systematic way of simplifying the computation. (2) We derive an efficient solution to the problem via constraint sampling and automatic differentiation, extending the work of Kilbertus et al. (2020b) to data of arbitrary dimension. (3) We illustrate our method on a range of synthetic and semi-synthetic datasets, where simulations confirm that our approach computes valid bounds even in complex settings where common assumptions fail.

The remainder of this paper is structured as follows. We formalize our problem setup in Section 2 and describe our solution in Section 3. Experimental results follow in Section 4. We conclude in Section 5 with a discussion of limitations and directions for future work.

2 Setup

We start by formulating the general setup and then provide two concrete running examples based on the IV model and a “leaky mediation” setting. Assume we observe data from causal model S^* that contains a potentially multivariate, continuous treatment $X \in \mathbb{R}^p$ and potentially continuous outcome $Y \in \mathbb{R}$ as observed variables, such that the true causal effect $o_{x^*}(S^*) := \mathbb{E}_{S^*}[Y | do(X = x^*)]$ is only partially (but not point-) identified.¹ Our goal will be to minimize/maximize this objective over all *admissible* causal models S among a (large) class of causal models \mathcal{S} . We characterize admissibility via two types of constraints. First, the missing edges of the assumed hidden variable directed acyclic graph (DAG) encode (conditional) independencies between variables. Further qualitative as-

¹We assume standard σ -algebras on these spaces. Further, we will assume throughout that all distributions have densities.

sumptions on the functional form of structural equations may be required for partial identification in certain settings. We refer to the constraints implied by graphical and functional assumptions jointly as *structural constraints*. Second, we have observational data from S^* . Denoting the (empirical) observed distribution by \hat{p} , the distribution p_S entailed by an admissible causal model S should replicate this distribution. We measure this *data constraint* via a distance function $\text{dist} : \mathcal{S} \times \mathcal{S} \rightarrow \mathbb{R}^+$ that measures the discrepancy between the joint distribution implied by a model $S \in \mathcal{S}$ and the observed data from the ground truth model S^* .² Hence, we arrive at the following general problem setting for computing the minimum/maximum causal effect among all models \mathcal{S} that are (dist, ϵ) -compatible with the observed data:

$$\min / \max_{S \in \mathcal{S}} o_{x^*}(S) \quad [\text{obj}] \quad (1)$$

$$\text{subject to } \text{dist}(p_S, \hat{p}) \leq \epsilon, \quad [\text{c-data}] \quad (2)$$

$$\text{struct. constraints} \quad [\text{c-struct}] \quad (3)$$

Note that, unlike most optimization objectives in machine learning, the objective in Equation (1) does not (directly) depend on the data. Instead, we optimize over models given another model (\hat{p}) as input; data only enters as constraints on which causal models are eligible. This suggests an interpretation of our task as decoupling model selection from model fitting: the former is a search over an *equivalence class* of causal models that (approximately) match the observable distribution. The latter is in the realm of standard machine learning, which produces (functionals of) \hat{p} regardless of causal assumptions. We believe this to be a fruitful viewpoint for a large variety of problems in causal inference that require us to simultaneously accommodate different qualitative structural assumptions and provide a good fit to observed data. Instead of conflating regularization and causal specification when no unique causal model explains the data (implying likelihood functions full of high-dimensional plateaus), our formulation considers all models in reasonable agreement with the estimated observable distribution. Moreover, as we show later, we can pick distance functions such that no density estimation problem has to be solved.

Consider the **instrumental variable** model in Figure 1a. We observe instruments $Z \in \mathcal{Z} \subset \mathbb{R}^q$, treatments $X \in \mathcal{X} \subset \mathbb{R}^p$, and outcomes $Y \in \mathcal{Y} \subset \mathbb{R}$ with a potentially high-dimensional unobserved confounder U between X and Y . Here we assume (A1) $X \not\perp\!\!\!\perp Z$, (A2) $Z \perp\!\!\!\perp \{U_X, U_Y\}$, and (A3) $Z \perp\!\!\!\perp Y | \{X, U_X, U_Y\}$. We denote the i.i.d. observations that make up \hat{p} by $\mathcal{D} = \{x_i, y_i, z_i\}_{i=1}^n$. Instead of the common additive noise or linearity assumptions, we consider a larger class of potentially *non-linear, non-additive* functions $f : \mathcal{X} \times \mathcal{U}_Y \rightarrow \mathcal{Y}, g : \mathcal{Z} \times \mathcal{U}_X \rightarrow \mathcal{X}$ that we will later encode in \mathcal{S} . We will propose to avoid full density estimation for [c-data] and instead only estimate $X | Z$ and the first two moments of $Y | X, Z$.

²We overload notation slightly by writing $\text{dist}(S, S^*) = \text{dist}(p_S, \hat{p})$, implicitly assuming dist can be evaluated on empirical distributions.

In the **leaky mediation** setting in Figure 1d., a second confounder between M and Y is added to the standard non-parametrically identified mediation example for front-door adjustment (Pearl, 2009, Ch. 3), rendering the causal effect of X on Y unidentifiable. Here, we have the structural constraints (B1) $X \perp\!\!\!\perp Y | \{M, U_Y\}$ and (B2) $U_X \perp\!\!\!\perp U_M$, and again allow for *non-linear, non-additive* functions $f : \mathcal{M} \times \mathcal{U}_Y \rightarrow \mathcal{Y}$, $g : \mathcal{X} \times \mathcal{U}_M \rightarrow \mathcal{M}$.

Requirements. The key difficulty in operationalizing the optimization in Equation (1) is the parameterization of \mathcal{S} . Our design choices are guided by efficiency of (i) the (constrained) optimization of $o_{x^*}(S)$, (ii) the evaluation of $\text{dist}(p_S, \hat{p})$, (iii) restricting \mathcal{S} to causal models satisfying **[c-struct]**. Moreover, we explicitly aim for methods that scale to large sample sizes n as well as multivariate treatments ($p > 1$) and instruments/mediators ($q > 1$).

Remarks. Before describing our bounding method in detail, we make the following observations. Increasing the capacity of \mathcal{S} will generally lead to wider, less informative bounds. Similarly, increasing the tolerance ϵ or reducing the sensitivity of the similarity measure dist will also lead to less informative bounds. While the structural constraints **[c-struct]** are strictly required to obtain valid bounds, relaxing or approximating the data constraints **[c-data]** may lead to wider—but never theoretically invalid—bounds.

3 Method

We now describe how we implement our framework.

3.1 Graphical reduction

To begin, we reduce a given graphical structure to a form that simplifies computation and removes any unnecessary assumptions. Figure 1 illustrates the following reduction steps for IV and leaky mediator examples.

- Imagine we are given a graph that explicitly includes the latent background variables U of a *structural causal model* (Pearl, 2009), where each observed variable is a deterministic function of its direct causes. We express unmeasured confounding with bidirected edges among the background variables. This forms a model of *marginal independence* (Richardson, 2003) among U variables, which can be hard to parameterize.
- To simplify computation, we convert as many bidirected edges to directed edges as possible while preserving the same structural constraints (Drton and Richardson, 2008). This allows for a simplified parameterization. For instance, for the leaky mediator we have $p(u_x, u_m, u_y) = p(u_x) p(u_m) p(u_y | u_x, u_m)$.
- We can remove unnecessary assumptions about structural equations when $p(v | do(\text{pa}(v)))$, the distribution of some variable V under intervention on its parents $\text{pa}(V)$, is *identifiable*. Instead of treating U_V as structural background variables with an unknown distribution and dimensionality, we convert them into

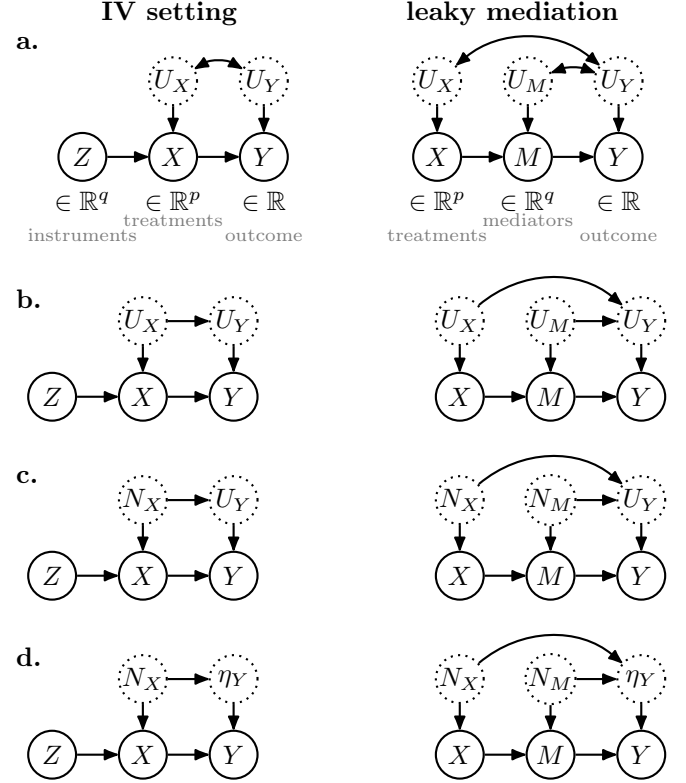


Figure 1: We show the general graphical reduction procedure for modeling latent confounding described in the text for the IV and leaky mediation setting.

“non-causal” scalar random variables N_V with a fixed distribution so that V is a deterministic function of its parents, which is invertible on N_V . For instance, we can model $p(x | z, u_x)$ in the IV model as $X = F_{X|Z}^{-1}(N_X)$, where $F_{X|Z}(\cdot)$ is the cdf of X given Z and N_X is uniform on $[0, 1]$.

- Finally, any remaining background variable will require further causal assumptions. In the sequel, we describe how we can recast the conditional model for each variable V with a parent U_V as being generated by a mixture of deterministic functions.

All of the above provides an alternative to blackbox models such as Hu et al. (2021), which ignore that many of the assumptions about structural equations can be avoided, and that many factors of the data distribution can be directly encoded without wasteful Monte Carlo simulations.

3.2 Response function framework

We now introduce a computational simplification on unobserved variables (the following is described with respect to the IV model; similar logic applies in the leaky mediator setting). First, note that specifying a causal model S as depicted in Figure 1a. involves the functions f and g , as well as the distribution of the potentially infinite dimensional confounder $U = \{U_X, U_Y\}$. To reduce this complexity, we make use of the so-called *response function* framework (Balke and Pearl, 1994; Kilbertus et al., 2020b). We call $f(\cdot, u) := f_u(\cdot) : \mathcal{X} \rightarrow \mathcal{Y}$ the response function for

the fixed value $U = u$ of the confounder. Note that in this case, f_u indeed encodes the direct causal effect of X on Y . A distribution over values of U entails a distribution over response functions f_u . Hence, instead of explicitly modeling U and f separately as part of a causal model S , we can directly encode them jointly via a distribution over response functions.

Without restrictions on the functional dependence of X and Y on U , one cannot obtain non-trivial bounds (Gundersius, 2021, 2019). As in general we have little information about the dimensionality and distribution of U , we argue that it is more practical to work with the equivalent assumptions on the function space and distribution of response functions f_u .

Specifically, we choose a family of response functions $\mathcal{F} \subset \{f : \mathcal{X} \rightarrow \mathcal{Y}\}$ that captures plausible direct causal effects from X to Y under all possible values of the confounding variable(s). We then assume a parameterized family of distributions over \mathcal{F} , denoted by $\{p_\eta^\mathcal{F} \mid \eta \in \mathbb{R}^d\}$. For concreteness, in our experiments we work with parameterized response functions as linear combinations of a set of non-linear basis functions $\{\psi_k : \mathcal{X} \rightarrow \mathcal{Y}\}_{k=1}^K$ for some $K \in \mathbb{N}$:

$$\mathcal{F} := \left\{ f_\theta := \sum_{k=1}^K \theta_k \psi_k \mid \theta_k \in \mathbb{R} \right\}. \quad (4)$$

Hence, once \mathcal{F} is fixed, $p_\eta^\mathcal{F}$ is fully described as a distribution over $\theta \in \mathbb{R}^K$. For ease of notation, we often drop the dependence on \mathcal{F} and summarize $\psi := (\psi_1, \dots, \psi_K)$.

3.3 Parameterizing \mathcal{S} and satisfying [c-struct]

Next, we describe how to leverage the response function framework for a useful parameterization of causal models \mathcal{S} . Again, we focus on the IV case for concreteness; see Appendix A for our analysis of the leaky mediator setting.

Despite recent advances in adding exact (conditional) independencies [c-struct] as explicit constraints in a smooth gradient-based optimization (Zheng et al., 2018), this approach is still unwieldy in our case with unobserved confounding. Therefore we encode [c-struct] directly in our choice of model class \mathcal{S} and write for clarity

$$\bar{\mathcal{S}} := \{p_\eta \mid \eta \in \mathbb{R}^d; (\text{A1})\text{-(A3)} \text{ satisfied for } (X, Y, Z) \sim p_\eta\}.$$

Using the parameterization from Equation (4), we may now reformulate (A2) and (A3) as $Z \perp\!\!\!\perp \theta$ and $Z \not\perp\!\!\!\perp \theta \mid X$. Consequently, we propose the DAG in Figure 1b. as a model for θ that explicitly encodes (A2) and (A3) via d -separation (Pearl, 2009). Hence, when basing all $p_\eta \in \bar{\mathcal{S}}$ on this graphical structure, we have absorbed [c-struct] into the definition of $\bar{\mathcal{S}}$. We think of N as a source of randomness that is shared in modeling $X \mid \{Z, N\}$ and $\theta \mid N$, thereby still allowing for dependencies between X and θ . Observe that a model for $X \mid \{Z, N\}$ can be fit once

upfront from observed data and remains fixed throughout the optimization. Later, we will need to deterministically recover N from Z and X , leaving us with any invertible conditional model $h_Z(N)$ for which $h_{Z=z}^{-1}(x)$ exists uniquely for all $z \in \mathcal{Z}$ and $x \in \mathcal{X}$. For example, conditional normalizing flows composed of invertible and differentiable (i.e., diffeomorphic) transformations (Papamakarios et al., 2021) are flexible candidates that we use in our experiments. Note that this parameterization implies $d_N = p$. We provide all details of the specific implementation in Appendix E.

Once h_Z is fixed, we model θ as a multivariate Gaussian via

$$\theta \mid N \sim \mathcal{N}(\mu_{\eta_0}(N), \Sigma_{\eta_1}(N)), \quad (5)$$

with mean and covariance functions $\mu_{\eta_0}(N)$ and $\Sigma_{\eta_1}(N)$, both parameterized by our optimization parameters $\eta = (\eta_0, \eta_1)$. To ensure $\Sigma_{\eta_1}(N)$ is a valid covariance matrix, we represent it in terms of its Cholesky factor L and add a small constant Ω to the diagonal $\Sigma_{\eta_1} = L^\top L + \Omega \mathbf{1}\mathbf{1}^\top$. Again we can use flexible function approximators for μ_{η_0} and Σ_{η_1} and resort to neural networks with parameters η_0 and η_1 in our experiments. The combined parameters $\eta = (\eta_0, \eta_1)$ now encode our family of causal models $\bar{\mathcal{S}} = \{p_\eta \mid \eta \in \mathbb{R}^d\}$, where Y is implicitly given by the random variable $f_\theta(X)$ with $X = h_Z(N)$, $N \sim \mathcal{N}(\mathbf{0}, \mathbf{1})$, and $\theta \mid N$ as in Equation (5). We remark that instead of the parameterization in Equation (5), we could have used any of a large class of flexible models such as mixture density networks or flow-based models. Our implementation choices were largely motivated by simplicity of exposition.

We now rephrase our main optimization problem as:

$$\begin{aligned} \min_{\eta \in \mathbb{R}^d} / \max_{\eta \in \mathbb{R}^d} & o_{x^*}(\eta) = \psi(x^*)^\top \mathbb{E}_N[\mu_{\eta_0}(N)] \quad [\text{obj}] \\ \text{subject to} & \text{dist}(p_\eta, \hat{p}) \leq \epsilon. \quad [\text{c-data}] \end{aligned}$$

For the objective equation, we used the law of total expectation. Since N follows a standard Gaussian, we can easily estimate the remaining expectation from a finite sample. So far, the data have only entered once when we chose $\bar{\mathcal{S}}$ such that $\hat{p}(X \mid Z)$ is matched by all $p_\eta \in \bar{\mathcal{S}}$. We still must enforce the remaining data matching constraints [c-data].

3.4 Satisfying [c-data]: matching the data

We first factor $p(Z, X, Y) = p(Y \mid X, Z) p(X \mid Z) p(Z)$. A key advantage of our construction of $\bar{\mathcal{S}}$ is that we only need to match the factor $p(Y \mid X, Z)$ to satisfy [c-data] instead of having to perform density estimation to match high-dimensional distributions via, e.g., f-divergences, integral probability metrics, Stein discrepancy, adversarial optimization, or variational inference. For us, any efficiently computable similarity measure dist on $\hat{p}(Y \mid X, Z)$ and $f_\theta(X) \mid \{X, Z\}$ can be used to keep candidate models p_η close to matching the *entire* observed data distribution. This matching can conveniently be formulated quite literally as matching expectations of the two distributions

Algorithm 1 Computing upper or lower bounds on $\mathbb{E}[Y \mid do(X = x^*)]$ in the IV setting.

Require: dataset $\mathcal{D} = \{(z_i, x_i, y_i)\}_{i=1}^n$; constraint functions $\{\phi_l : \mathcal{Y} \rightarrow \mathbb{R}\}_{l=1}^L$; basis functions $\{\psi_k : \mathcal{X} \rightarrow \mathcal{Y}\}_{k=1}^K$; norm $\|\cdot\|$ for dist; batchsize for Monte Carlo B ; number of support points M ; tolerance $\epsilon > 0$

Setup: One-time computations shared for different x^* values

- 1: Fit (invertible) conditional normalizing flow $X = h_Z(N)$ from data \mathcal{D} for $N \sim \mathcal{N}(0, \mathbf{1}_p)$ \triangleright fix $X \mid Z$ model
- 2: Fit MLPs $\hat{\phi}_1 : x_i, z_i \rightarrow y_i$ and $\hat{\phi}_2 : x_i, z_i \rightarrow y_i^2$ by minimizing the squared loss from data \mathcal{D} \triangleright fix constraint targets
- 3: subsample M indices uniformly without replacement from $[n]$ \triangleright “support points”, assume w.l.o.g. those are $[M]$

Optimization: performed separately for lower and upper bound for each x^*

- 4: minimize OBJECTIVE(η) subject to CONSTRAINT(η) $\leq \epsilon$ using augmented Lagrangian (see Appendix E.4 for details)

- 5: **function** OBJECTIVE(η)
- 6: $o_{x^*}(\eta) \leftarrow \psi(x^*)^\top \frac{1}{B} \sum_{j=1}^B \mu_{\eta_0}(n_j)$ with $n_j \sim \mathcal{N}(0, \mathbf{1}_p)$ \triangleright differentiable w.r.t. η
- 7: **return** $\pm o_{x^*}(\eta)$ \triangleright objective, \pm for lower/upper bound

- 8: **function** CONSTRAINT(η)
- 9: $n_j \leftarrow h_{z_j}^{-1}(x_j)$ for $j \in [M]$ \triangleright invert $X \mid Z$ model to infer “noises”
- 10: $A_{1,j}(\eta) \leftarrow \psi(x_j)^\top \mu_{\eta_0}(n_j)$ for $j \in [M]$ \triangleright first moments implied by model
- 11: $A_{2,j}(\eta) \leftarrow \psi(x_j)^\top (\Sigma_{\eta_1}(n_j) + \mu_{\eta_0}(n_j)\mu_{\eta_0}(n_j)^\top) \psi(x_j)$ for $j \in [M]$ \triangleright second moments implied by model
- 12: $\nu_{l,j} \leftarrow \hat{\phi}_l(x_j, z_j) - A_{l,j}(\eta)$ for $l \in \{1, 2\}, j \in [M]$ \triangleright constraint matrix
- 13: **return** $\|\nu\|$

when transformed by a fixed set of dictionary functions $\{\phi_l : \mathcal{Y} \rightarrow \mathbb{R}\}_{l=1}^L$. That is, we want the absolute values of

$$\nu_l(x, z) = \mathbb{E}_{y \sim \hat{p}(y \mid x, z)}[\phi_l(y)] - \mathbb{E}_{\theta \sim p_\eta(\theta \mid x, z)}[\phi_l(f_\theta(x))], \quad (6)$$

to be small for all l and all $(x, z) \in \mathcal{X} \times \mathcal{Z}$. Since X, Z are continuous (and potentially high-dimensional), this would amount to an uncountably infinite set of constraints. In high dimensions, a naïve discretization of X, Z also fails (Kilbertus et al., 2020b). Instead, we aim to make $|\nu_l(x, z)|$ small at a representative, finite set of points in $\mathcal{X} \times \mathcal{Z}$. Arguably, the most representative set is a uniformly random subsample of the observed data \mathcal{D} of size M . For notational simplicity, we assume w.l.o.g. that these “support points” are the first M indices. In other words, defining (by some overloading of notation) the matrix $\nu \in \mathbb{R}^{L \times M}$ via $\nu_{l,j} = \nu_l(x_j, z_j)$ (using $j = 1, \dots, M$ to index the selected support points), we obtain a natural family of overall distances $\text{dist}(p_\eta, \hat{p}) = \|\nu\|$ for any (semi-)norm $\|\cdot\|$ on $\mathbb{R}^{L \times M}$.³ In our experiments, we specifically consider the entry-wise sup-norm $\|\cdot\|_{\infty, \infty}$ and the entry-wise 2-norm $\|\cdot\|_{2,2}$. For $\|\cdot\|_{\infty, \infty}$ we require the absolute value of each entry to be small, i.e., practically have to enforce $L \cdot M$ constraints, whereas for $\|\cdot\|_{2,2}$ we get away with a single overall constraint.

The **first expectation** in Equation (6) is estimable from the observed data via $\hat{\phi}_l(x, z) \approx \mathbb{E}[\phi_l(Y) \mid x, z]$, where

³We remark that, formally, if we allow $L, M \rightarrow \infty$ the functions ϕ_l can be chosen such that exact matching between \hat{p} and p_η can be approximated arbitrarily well, e.g., by approximating the characteristic function using l and matching it everywhere on $\mathcal{X} \times \mathcal{Y}$ using the entry-wise sup-norm.

$\hat{\phi}_l : \mathcal{X} \times \mathcal{Z} \rightarrow \mathbb{R}$ are regression functions mapping $x, z \rightarrow \mathbb{E}[\phi_l(Y) \mid x, z]$ that were learned in a supervised fashion on the training data \mathcal{D} . Because h_Z was assumed to be invertible, our modeling choice for $\bar{\mathcal{S}}$ plays nicely with our constraint formulation, in that we can explicitly write

$$p_\eta(\theta \mid x, z) = \mathcal{N}\left(\mu_{\eta_0}(h_z^{-1}(x)), \Sigma_{\eta_1}(h_z^{-1}(x))\right). \quad (7)$$

For general dictionary functions ϕ_l , we can again estimate the **second expectation** in Equation (6) using finite samples from Equation (7). To simplify optimization, in practice it often suffices to constrain the first few moments of $Y \mid \{X, Z\}$, e.g., to set $\phi_1(Y) = Y$ and $\phi_2(Y) = Y^2$. This task is much more data efficient than modeling the complete joint distribution $p(X, Y, Z)$, as required, for example, by generative methods such as GANs (Hu et al., 2021). We remark that because heteroskedastic Gaussians are maximum entropy distributions with fixed first and second moments, this set of dictionary functions matches our prior modeling choices with maximal flexibility. This further simplifies the second expectation in Equation (6) to the following:

$$A_{1,j}(\eta) = \psi(x_j)^\top \mu_{\eta_0}(n_j), \quad (8)$$

$$A_{2,j}(\eta) = \psi(x_j)^\top (\Sigma_{\eta_1}(n_j) + \mu_{\eta_0}(n_j)\mu_{\eta_0}(n_j)^\top) \psi(x_j),$$

where $n_j := h_{z_j}^{-1}(x_j)$ for $j \in [M]$.

3.5 Solving the optimization

Taking all the steps from previous sections together, we have $\nu_{l,j} = \hat{\phi}_l(x_j, z_j) - A_{l,j}(\eta)$ and ultimately arrive at

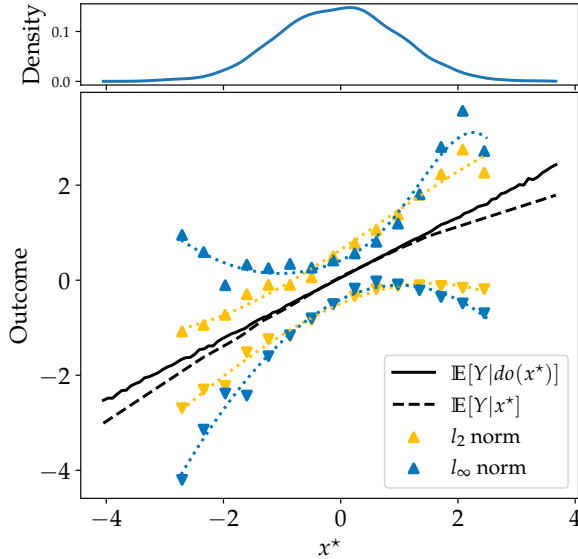


Figure 2: **IV-lin-2d-weak. Comparing norms** Our framework easily allows for different data-matching criteria (dist). The choices shown here ($\|\cdot\|_{\infty,\infty}$ and $\|\cdot\|_{2,2}$) yield comparable and consistent bounds.

the following non-convex optimization problem with non-convex constraints

$$\min_{\eta \in \mathbb{R}^d} / \max_{\eta \in \mathbb{R}^d} o_{x^*}(\eta) = \psi(x^*)^\top \mathbb{E}_N[\mu_{\eta_0}(N)] \quad [\text{obj}]$$

subject to $\|\nu\| \leq \epsilon$ [c-data]

for which the augmented Lagrangian method with inequality constraints is a natural choice (Nocedal and Wright, 2006, sec. 17.4). We provide a high-level description in Algorithm 1 and provide specifics in Appendix E.4. Note that for the entry-wise sup-norm $\|\cdot\|_{\infty,\infty}$ we aim at enforcing $M \cdot L$ inequality constraints, one for each entry. While we have already argued that $L = 2$ is a sensible choice, we get to choose a fixed number of “support data-points” M regardless of the dimensionality of X to trade off capturing the observed distribution and stability of the augmented Lagrangian optimization. For very high-dimensional data, one may take inspiration from Wang and Bertsekas (2016) and further subsample a fixed number of constraints uniformly at random at each step of the optimization. For convex problems, this form of constraint subsampling can be shown to converge to the optimal solution (Wang and Bertsekas, 2016). Finally, while our problem is not convex, we take the usual leap of faith and hope for convergence at least to a local minimum in the non-convex case and perform multiple restarts only keeping the largest (for maximization) or smallest (for minimization) value respectively.

4 Experiments

Since ground truth causal effects must be known to properly evaluate the validity of our bounds, we primarily make use of simulated datasets. All experiments in the

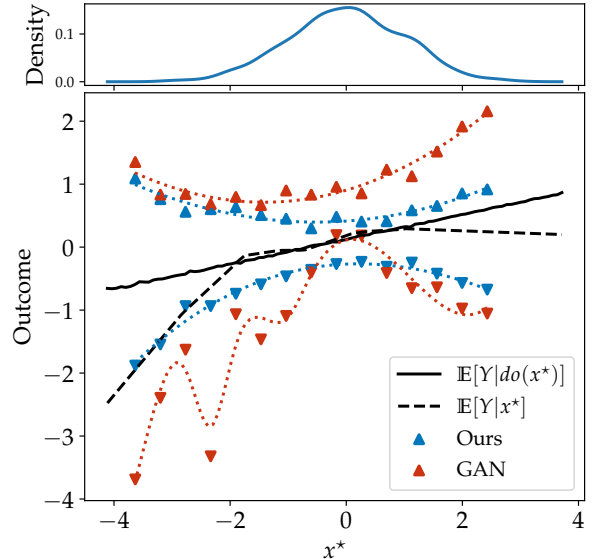


Figure 3: **LM-lin-2d-strong. Leaky mediator setting** We get reliable bounds also in the leaky mediator setting compared to the GAN framework.

main paper are in a partially identifiable setting. As a sanity check, we show experiments for identifiable settings as well as for other datasets and constraint formulations in Appendix F.

4.1 Treatment choices

When visualizing results for multidimensional treatments X , we vary the interventional values x^* along a single treatment dimension, keeping the remaining components at fixed values. While this allows us to show continuous treatment effect curves, we note our method can compute bounds for any multidimensional intervention $do(X = x^*)$. Specifically, in the results shown here, we vary the first component of X and fix the values of the other components to their empirical marginal means. For each figure, we include a kernel density estimate of the marginal distribution of the empirically observed treatments to distinguish “data poor” from “data rich” regions. In “data poor” regions (towards the tails of the empirical distribution), we may expect our bounds to become looser, as less information about the data-matching constraints is available.

4.2 Baselines

We compare our method to a naïve regression and the method of Hu et al. (2021).

- **Regression with MLP.** We naïvely fit an MLP with quadratic loss to predict outcome Y from the multi-dimensional treatment X , a modeling approach that assumes no confounding at all.
- **GAN framework.** Hu et al. (2021) parameterize the causal model (i.e., its exogenous random variables and structural equations) with neural networks and apply

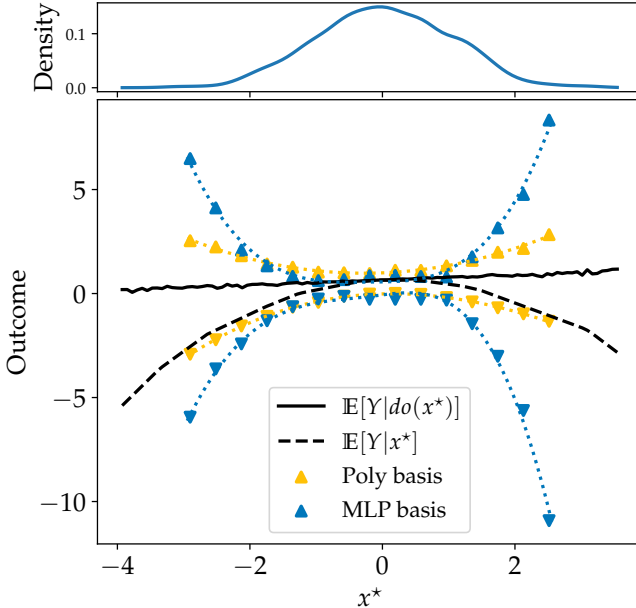


Figure 4: **IV-lin-2d-strong: Comparing response functions.** As expected, neural response functions give wider bounds than a linear polynomial basis because of being less expressive.

the adversarial learning framework to search the parameter space. We adjust the model in their code to our examples, but otherwise leave hyperparameter choices and convergence criteria untouched. The error allowed on matching the observed distribution is $\eta = 0.001$ (not our η) and bounds are calculated as the mean over the effects of the 50 last models with error below η , plus/minus the variance of those 50 values.

4.3 Implementation choices

Choice of response functions. As described in Equation (4), we choose linear combinations of non-linear basis functions $\{\psi_k\}_{k \in [K]}$. For our experiments we mostly work with a set of K *neural basis functions*, obtained from the last hidden-layer activations of an MLP fit to the observed data $\{(x_i, y_i)\}_{i \in [n]}$, as well as (multivariate) polynomials up to a fixed degree (see Appendix D for details). For two-dimensional treatments, we use $K = 6$ and $K = 3$ for polynomial and neural basis functions, respectively. For three-dimensional treatments we use $K = 10$ for both polynomial and neural basis functions. This corresponds to using up to quadratic terms in the polynomial basis for both two- and three-dimensional treatments.

For our method, we individually compute **lower** (∇) and **upper** (Δ) bounds at multiple values $x^* \in \mathbb{R}$ for one dimension of the treatment and show how it compares to the **true causal effect** (—) and **naïve regression** (---). The lines shown for **lower** and **upper** (.....) bounds are univariate cubic splines fit to the bounds for individual x^* -grid values. We use $n = 10000$ i.i.d. sampled datapoints for each experiment and subsample $M = 100$ datapoints uniformly at random for the data constraints [c-data].

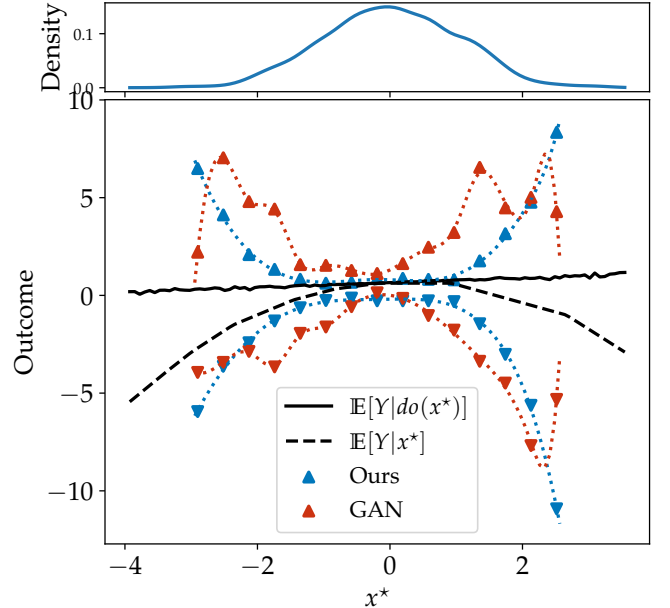


Figure 5: **IV-lin-2d-strong: GAN comparison.** Our method reliably yields valid bounds even under strong confounding, while the GAN framework becomes unstable, potentially due to the difficulties of solving a bilevel optimization problem.

For the $X | Z$ model in the IV setting we use a quadratic conditional spline normalizing flow. All other details of the implementation, including hyperparameter choices, are described in Appendix E.

Getting final bound estimates. For each x^* , we run 5 different optimizations starting with 5 different seeds each for the lower and upper bounds. For the final upper bound estimate, we take the maximum of the 5 upper bound estimates we get, and for the final lower bound estimate we take the minimum of the 5 lower bound estimates we get. We follow the same process for the GAN bounds.

4.4 Results

We focus on datasets where the true effect is a linear or quadratic polynomial function of the treatment X . A full glossary of datasets can be found in Appendix C, along with exact structural equations for each setting. While the naming of the datasets is intuitive, Figure 7 provides a short description of the naming logic. We now describe the results obtained for selected datasets with more results and details in Appendix F.

IV-lin-2d-strong. This dataset is simulated from an IV setting, where the true effect $Y | do(X)$ is linear in a two-dimensional treatment X . The naïve regression $\mathbb{E}[Y | X]$ differs substantially from the true effect, indicating strong confounding (see, Figure 4).

We start by assessing the effect of the flexibility of response functions on our bounds in Figure 4. Choosing less flexible basis functions (polynomials) yields tighter bounds, highlighting the flexibility of our approach in

obtaining more informative bounds when more restrictive assumptions are being made. Our method can also accommodate alternative constraint formulations and slack parameters. We show experiments demonstrating this flexibility in Appendix F. While sometimes loose, especially for flexible basis functions (MLP) and in “data poor” regions towards the tails of the empirical distribution of observed treatments, our bounds contain the true causal effect for all x^* . This validity of our bounds holds up for all other experiments as well.

Next, Figure 5 compares our approach to the GAN framework baseline. First, we note that methods that fit a model and bounds at the same time, like Hu et al. (2021), essentially need to solve a bilevel optimization problem, where the same parameters are shared in the definition of the constraints (which require optimizing a measure of fitness) and the causal quantity of interest (which requires optimizing a different problem). Such a strategy can be wasteful and potentially more prone to optimization and regularization challenges. Our goal in comparing⁴ to Hu et al. (2021) is to show that our framework can exploit structure to reduce which constraints to numerically enforce, avoids full density estimation, while giving comparable or arguably better results than those from the GAN framework. Indeed, Figure 5 shows that despite the flexible neural basis functions, our approach can yield tighter bounds and mostly avoid instabilities as observed for the GAN approach when we move towards the tails of the observed distribution.

We show similar comparisons for linear and quadratic true effect IV settings with strong and weak confounding as well as two- and three-dimensional treatments in Appendix F.

IV-lin-2d-weak. This is an IV setting with weak confounding. In Figure 2 we show how our bounds behave under different choices of dist, namely under the entry-wise $\|\cdot\|_{\infty,\infty}$ norm (which results in $M \cdot L$ constraints in the augmented Lagrangian) versus the entry-wise $\|\cdot\|_{2,2}$ norm (yielding only a single constraint). The obtained bounds are compatible and comparable, indicating relatively mild effects of the choice of the data-matching criterion dist.

LM-lin-2d-strong. Figure 3 shows results for data from a leaky mediator setting, where the true effect is a linear function of the mediator M , and the treatment X is two-dimensional. Confounding between the mediator and the effect is relatively strong. These results corroborate our findings regarding stability and reliability of our bounds compared to the GAN framework from the IV setting, despite using the neural basis function. Again, additional results for different structural assumptions, treatment dimensions, and confounding strength are presented in Appendix F.

⁴For generality, we use the *neural basis functions* for all experiments where we compare to the GAN framework, as they are expected to give wider bounds than polynomials.

5 Discussion

Causal modeling inevitably involves a trade-off between the strength of input assumptions and the specificity of resulting inferences. Our approach is no exception, meaning that it critically relies on untestable structural assumptions. Misspecification of $\bar{\mathcal{S}}$, which occurs when the true data generating model S^* is not in $\bar{\mathcal{S}}$, could lead our procedure to produce invalid bounds. In practice, a sufficiently rich class of causal models may contain the true causal effect even when $S^* \notin \bar{\mathcal{S}}$; however, we cannot guarantee this. After parameterization, the optimization problem in Equation (1) will generally result in a *non-convex objective with non-convex constraints*. Therefore, our proposed gradient-based local optimization may not converge to a global optimum, rendering our bounds overly tight. Empirically, we do not observe evidence of consistently getting stuck in bad local optima. Because we optimize both bounds individually for each value of x^* , our method may be computationally expensive when the intervention space is very large. However, it is well-suited for scenarios where we want reliable bounds on a well-defined set of plausible interventions. Finally, we have not accounted for the uncertainty of our bounds. Confidence or credible intervals for both extrema can help practitioners evaluate the reliability of causal inferences and are an interesting direction for future work.

We observe that our procedure can additionally be used to evaluate whether causal effects are identifiable under some plausible equivalence class of DAGs. In this respect, the method instantiates a version of the algorithm described by Xia et al. (2021, Alg. 1), which they show to be sound and complete for effect identification with a class of neural causal models. However, whereas their description is quite abstract, we find that parameterization details inevitably vary across different graphical structures. By working through the details of bounding in the IV and leaky mediator settings with continuous, multivariate data, we attempt to illustrate how such an approach can work in practice.

We have introduced a stochastic causal program for bounding treatment effects in partially identifiable settings. Our approach does not rely on the typical assumptions of linearity, monotonicity, or additivity. We presented a novel parameterization for decoupling observed from unobserved potential outcomes, and derived an efficient procedure for optimizing over a set of causal models consistent with the data. Experiments demonstrate that our method produces valid and informative bounds in a wide range of settings, including with continuous and multidimensional instruments, mediators, treatments, and outcomes.

6 Acknowledgments

This work was partially supported by ONR grant 62909-19-1-2096 to RS. This work was supported by the UKRI [grant number EP/S021566/1].

References

Angrist, J. D. and Imbens, G. W. (1995). Two-stage least squares estimation of average causal effects in models with variable treatment intensity. *J. Am. Stat. Assoc.*, 90(430):431–442.

Balke, A. and Pearl, J. (1994). Counterfactual probabilities: Computational methods, bounds and applications. In *Proceedings of the 10th Conference on Uncertainty in Artificial Intelligence*, pages 46–54.

Balke, A. and Pearl, J. (1997). Bounds on treatment effects from studies with imperfect compliance. *J. Am. Stat. Assoc.*, 92(439):1171–1176.

Bennett, A., Kallus, N., and Schnabel, T. (2019). Deep generalized method of moments for instrumental variable analysis. In *Advances in Neural Information Processing Systems*.

Bica, I., Alaa, A. M., Lambert, C., and van der Schaar, M. (2021). From real-world patient data to individualized treatment effects using machine learning: Current and future methods to address underlying challenges. *Clin. Pharmacol. Ther.*, 109(1).

Bingham, E., Chen, J. P., Jankowiak, M., Obermeyer, F., Pradhan, N., Karaletsos, T., Singh, R., Szerlip, P. A., Horsfall, P., and Goodman, N. D. (2019). Pyro: Deep universal probabilistic programming. *J. Mach. Learn. Res.*, 20:28:1–28:6.

Chernozhukov, V., Chetverikov, D., and Kato, K. (2018). Inference on causal and structural parameters using many moment inequalities. *Rev. Econ. Stud.*, 86(5):1867–1900.

Chickering, D. M. and Pearl, J. (1996). A clinician’s tool for analyzing non-compliance. In *Proceedings of the 13th AAAI Conference on Artificial Intelligence*, pages 1269–1276.

Daubechies, I., DeVore, R., Foucart, S., Hanin, B., and Petrova, G. (2021). Nonlinear approximation and (deep) relu networks. *Constr. Approx.*, pages 1–46.

Drton, M. and Richardson, T. (2008). Graphical methods for efficient likelihood inference in Gaussian covariance models. *J. Mach. Learn. Res.*, 9:893–914.

Fisher, R. A. (1957). Dangers of Cigarette-smoking. *BMJ*, 2(5039):297–298.

Franks, A., D’Amour, A., and Feller, A. (2019). Flexible sensitivity analysis for observational studies without observable implications. *J. Am. Stat. Assoc.*

Gunsilius, F. (2019). Bounds in continuous instrumental variable models. *arXiv* preprint, 1910.09502.

Gunsilius, F. F. (2021). Nontestability of instrument validity under continuous treatments. *Biometrika*, 108(4):989–995.

Hartford, J., Lewis, G., Leyton-Brown, K., and Taddy, M. (2017). Deep IV: A flexible approach for counterfactual prediction. In *Proceedings of the 34th International Conference on Machine Learning*.

Hu, Y., Wu, Y., Zhang, L., and Wu, X. (2021). A generative adversarial framework for bounding confounded causal effects. In *Proceedings of the 35th AAAI Conference on Artificial Intelligence*.

Imbens, G. W. and Rubin, D. B. (2015). *Causal Inference for Statistics, Social, and Biomedical Sciences: An Introduction*. Cambridge University Press, Cambridge.

Kallus, N. and Zhou, A. (2020). Confounding-robust policy evaluation in infinite-horizon reinforcement learning. In *Advances in Neural Information Processing Systems*.

Kilbertus, N., Ball, P. J., Kusner, M. J., Weller, A., and Silva, R. (2020a). The sensitivity of counterfactual fairness to unmeasured confounding. In *Proceedings of The 35th Conference on Uncertainty in Artificial Intelligence*, pages 616–626.

Kilbertus, N., Kusner, M. J., and Silva, R. (2020b). A class of algorithms for general instrumental variable models. In *Advances in Neural Information Processing Systems*.

Manski, C. F. (1990). Nonparametric bounds on treatment effects. *Am. Econ. Rev.*, 80(2):319–323.

Muandet, K., Mehrjou, A., Lee, S. K., and Raj, A. (2020). Dual instrumental variable regression. In *Advances in Neural Information Processing Systems*, volume 33, pages 2710–2721.

Nocedal, J. and Wright, S. (2006). *Numerical optimization*. Springer Science & Business Media.

Papamakarios, G., Nalisnick, E., Rezende, D. J., Mohamed, S., and Lakshminarayanan, B. (2021). Normalizing flows for probabilistic modeling and inference. *J. Mach. Learn. Res.*, 22(57):1–64.

Paszke, A., Gross, S., Massa, F., Lerer, A., Bradbury, J., Chanan, G., Killeen, T., Lin, Z., Gimelshein, N., Antiga, L., Desmaison, A., Kopf, A., Yang, E., DeVito, Z., Raison, M., Tejani, A., Chilamkurthy, S., Steiner, B., Fang, L., Bai, J., and Chintala, S. (2019). Pytorch: An imperative style, high-performance deep learning library. In *Advances in Neural Information Processing Systems 32*, pages 8024–8035.

Pearl, J. (2009). *Causality*. Cambridge University Press, New York.

Richardson, T. (2003). Markov properties for acyclic directed mixed graphs. *Scand. J. Stat.*, 30(1):145–157.

Saltelli, A. (2002). Sensitivity Analysis for Importance Assessment. *Risk Anal.*, 22(3):579–590.

Shen, Z., Yang, H., and Zhang, S. (2021). Neural network approximation: Three hidden layers are enough. *Neural Netw.*, 141:160–173.

Shpitser, I. and Pearl, J. (2008). Complete identification methods for the causal hierarchy. *J. Mach. Learn. Res.*, 9:1941–1979.

Singh, R., Sahani, M., and Gretton, A. (2019). Kernel instrumental variable regression. In *Advances in Neural Information Processing Systems*, pages 4595–4607.

Vandenbroucke, J. P., Broadbent, A., and Pearce, N. (2016). Causality and causal inference in epidemiology: the need for a pluralistic approach. *Int. J. Epidemiol.*, 45(6):1776–1786.

Wang, M. and Bertsekas, D. P. (2016). Stochastic first-order methods with random constraint projection. *SIAM J. Optim.*, 26(1):681–717.

Wu, Y., Zhang, L., and Wu, X. (2019a). Counterfactual fairness: Unidentification, bound and algorithm. In *Proceedings of the 28th International Joint Conference on Artificial Intelligence*, pages 1438–1444.

Wu, Y., Zhang, L., Wu, X., and Tong, H. (2019b). Pcfairness: A unified framework for measuring causality-based fairness. In *Advances in Neural Information Processing Systems*.

Xia, K., Lee, K.-Z., Bengio, Y., and Bareinboim, E. (2021). The neural-causal connection: expressiveness, learnability, and inference. In *Advances in Neural Information Processing Systems*.

Zhang, J. and Bareinboim, E. (2020). Designing optimal dynamic treatment regimes: A causal reinforcement learning approach. In *Proceedings of the 37th International Conference on Machine Learning*.

Zhang, J. and Bareinboim, E. (2021). Bounding causal effects on continuous outcomes. In *Proceedings of the 35th AAAI Conference on Artificial Intelligence*.

Zheng, X., Aragam, B., Ravikumar, P. K., and Xing, E. P. (2018). Dags with no tears: Continuous optimization for structure learning. In *Advances in Neural Information Processing Systems 31*.

A Leaky mediator

In the “leaky mediator” setup, we have that the effect of treatment X on outcome Y is completely mediated by some vector M . On top of that, X and Y are confounded, and so are M and Y . Without the latter, this causal structure would satisfy the front-door criterion, and be nonparametrically identifiable via the do-calculus (Pearl, 2009). A causal diagram with our proposed parameterization is shown in Figure 1(d), right column.

For fixed background variables U_Y encoded indirectly as function parameters θ_y , the structural equation for Y is given by $f_{\theta_y}(m)$. Assume we represent the density function of M given X , $p_m(\cdot | x)$, with an invertible conditional normalizing flow $M = h_X(N_M)$, where $N_M \sim \mathcal{N}(0, 1)$. In what follows, we adopt no model for $p_x(x)$ ($= p(n_x)$), using its empirical distribution $\hat{p}_x(\cdot)$ as an estimate.

Representing the objective function. A main difference between this and the IV model is that we also need to marginalize the mediator M . We can interpret the expectation $\mathbb{E}[Y | do(x^*)]$ as following the same generative model of the observational distribution, but where node X gets replaced by constant x^* , with edge $N_X \rightarrow X$ also removed. This leads to the following integral and its Monte Carlo approximation:

$$\begin{aligned} \mathbb{E}[Y | do(x^*)] &= \int f_{\theta_y}(m)p(m, n_x, \theta_y | do(x^*)) dm dn_x d\theta_y \\ &\approx \frac{1}{n} \sum_i \theta_y^{(i)\top} \psi(m^{(i)}), \end{aligned} \quad (10)$$

where

$$\begin{aligned} n_x^{(i)} | do(x^*) &\sim \hat{p}_x(\cdot) \\ m^{(i)} | n_x^{(i)}, do(x^*) &\sim \hat{p}_m(\cdot | x^*) \\ n_m^{(i)} | m^{(i)}, do(x^*) &= h_{x^*}^{-1}(m^{(i)}) \\ \theta_y^{(i)} | n_m^{(i)}, m^{(i)}, n_x^{(i)}, do(x^*) &\sim p_\eta(\cdot | n_x^{(i)}, n_m^{(i)}) \end{aligned}$$

Here, n is the number of Monte Carlo samples; $\hat{p}_x(\cdot)$ is the empirical distribution of X (and, hence, sampling from it is just sampling with replacement from the training set for X). This can be interpreted conceptually, with the actual algorithm being the sampling of N_M from a standard Gaussian followed by the computation of M from x^* and N_M .

Estimating the constraints. Our optimization is over multivariate Gaussian distributions of θ_y with the mean and covariance modeled by MLPs with parameters η_0 and η_1 , respectively. Let’s say the MLPs are $\mu_{\eta_0}(n_x, n_m)$ and $\Sigma_{\eta_1}(n_x, n_m)$. The constraints of the optimization are to match the generated data to the observed distribution, for example by matching the first and second moments of $Y | X, M$ as in the IV case.

$$\mathbb{E}[Y | x, m] = \int f_{\theta_y}(m)p(\theta_y | x, m) d\theta_y \quad (11)$$

$$= \mathbb{E}[\theta^\top | x, m] \psi(m) \quad (12)$$

$$= \mu_{\eta_0}(x, n_m(x, m))^\top \psi(m) \quad (13)$$

This is analogous to the IV setting because of the similar factorization of the background variables as a DAG after re-encoding the bidirected edges as directed edges. After transforming the causal background variables U_X, U_M into probabilistic “seeds” N_X, N_M for $p(x)$ and $p(m | x)$, this results in the factorization $p(n_x)p(n_m)p(\theta_y | n_m, n_x)$. As N_X is identically distributed as X and so can be estimated separately, and $p(n_m)$ is fixed by design, the same general pipeline follows.

B Extensions

We introduced our problem formulation as a very generic definition of model proximity in terms of some $\text{dist}(p_\eta, \hat{p})$, and in particular the formulation

$$\text{dist}(p_\eta, \hat{p}) \equiv \|f^{p_\eta} - f^{\hat{p}}\|_\infty,$$

where $f^{\hat{p}}$ is a finite-dimensional vector of functionals of the (estimated) observable distribution, and f^{p_η} is a finite-dimensional vector of functionals of the distribution as implied by an unidentifiable structural causal model. Equation (6) is a particular implementation of this idea. Due to the challenge of evaluating this norm, we suggest Monte Carlo approximation for the optimization procedure, based on Wang and Bertsekas (2016).

We have also presented results for alternative distance metrics, including special cases such as metrics that can be associated with a single Lagrange multiplier such as $\|f^{p_\eta} - f^{\hat{p}}\|_2$. We note that also combinations of a limited number of metrics are possible such as

$$\max\{\|f_1^{p_\eta} - f_1^{\hat{p}}\|_1, \|f_1^{p_\eta} - f_2^{\hat{p}}\|_1, \dots, \|f_K^{p_\eta} - f_K^{\hat{p}}\|_1\},$$

where each $k = 1, 2, \dots, K$ describes a cluster of functionals that are easy to compare on the same scale.

We emphasize an approach where $f^{\hat{p}}$ is learned prior to solving an optimization problem. It may be of interest to use the raw data directly and try to fit p_η while searching, among all equally best fitting models, for the one with the highest/lowest corresponding causal effect. There are some appealing properties of using something like (Monte Carlo approximations of) the log-likelihood function evaluated at the training points (i.e., the negative KL divergence between model and data), maximum mean discrepancy measures, or generative adversarial network criteria, as they are global measures of goodness-of-fit. Future work on such approaches should also be considered. However, it is not entirely obvious how nested optimization would complicate the solution to the problem, as optimizing (and regularizing!) the fit plays the role of a constraint for the “true” objective function that is optimized (the causal effect). Moreover, fitting a generative model for the entire joint distribution is an obviously undesirable nuisance task if we can get essentially the same bounds by estimating only one or two moments of interest.

Another extension is the provision of a calculus for a minimal parameterization of arbitrary structural causal models for a given causal query of interest. Looking back at our

instrumental variable scenario, we could have created a single set of latent variables N_{XY} that would be common causes of X and Y and model the structural equations for both X and Y at the same time, instead of fixing $p(X | Z)$ a priori and deterministically extracting latent variables N from X and Z . In general, we could add independent latent variables for each clique in the bidirected graph component of the causal graph. This, however, is very wasteful. There is no need to create a causal model for the (Z, X) marginal – which not only would assume that Z is an unconfounded cause of X , which is unnecessary, but would also waste computation and stability trying to match the observable marginal of (Z, X) to the corresponding causal-model-implied marginal, which is also completely unnecessary. Given that Z and X can be high-dimensional while Y is a scalar, this is clearly a bad idea. Therefore, the structure-blind strategy of creating latent variables for each bidirected clique is convenient but not ideal, and a smarter automated way of generating minimal causal parameterizations for arbitrary graphs and causal queries is needed.

C Synthetic Datasets

C.1 Glossary of polynomial datasets

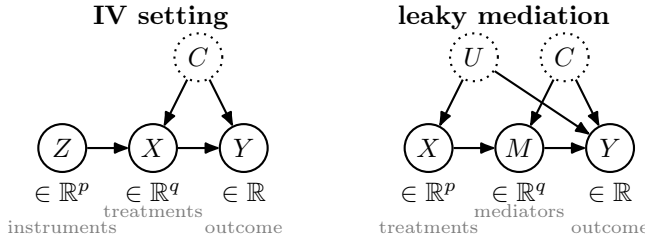


Figure 6: These are the structural equations we work with. In the description of the datasets, the dimensions of each variable are denoted by a subscript. For instance if X is 2-dimensional, we write it as $X = (x_1, x_2)$.

IV - lin - 2d - strong - add (optional)

Figure 7: Naming logic for the datasets. The *first* segment mentions whether it is the Instrument Variable (IV) or Leaky Mediator (LM) setting. The *second* segment says whether y is linear or quadratic in x . The *third* segment tells the dimension of the treatment. The *fourth* segment denotes the strength of the confounding, strong or weak. The *fifth* and last segment is optional, and says whether the confounding is additive, which in the IV setting makes the effect identifiable.

We use various polynomial datasets where the causal effect is a polynomial function of a single or multidimensional treatment. We provide the construction of each of these here. Figure 6 shows the structural graphs. In both graphs, every node except Y (outcome) could be multi-dimensional. If a node, say C , is multi-dimensional, we index the dimension with a subscript. That is, we write

$C = (c_1, c_2)$. Figure 7 visually describes the naming logic behind the datasets to make the exposition clearer.

Scalar treatment

We now describe settings where the treatment X is a scalar, which we present as a sanity check. The noises, confounder, and instrument follow

$$e_x, e_y, c, z \sim \mathcal{N}(0, 1)$$

IV-lin-1d-weak-add (f_y linear in x , weak additive confounding)

$$\begin{aligned} f_x(z, c, e_x) &= 3z + 0.5c + e_x \\ f_y(x, c, e_y) &= x - 6c + e_y \end{aligned}$$

IV-quad-1d-strong (f_y quadratic in x , strong non-additive confounding)

$$\begin{aligned} f_x(z, c, e_x) &= 0.5z + 3c + e_x \\ f_y(x, c, e_y) &= 0.3x^2 - 1.5xc + e_y \end{aligned}$$

IV-quad-1d-weak (f_y quadratic in x , weak non-additive confounding)

$$\begin{aligned} f_x(z, c, e_x) &= 3z + 0.5c + e_x \\ f_y(x, c, e_y) &= 0.3x^2 - 1.5xc + e_y \end{aligned}$$

IV model

We now describe datasets satisfying the IV assumptions.

2D treatment. The noises, confounder, and instruments follow

$$\begin{aligned} c, z, e_x &\sim \mathcal{N}^2(0, 1) \\ e_y &\sim \mathcal{N}(0, 1) \end{aligned}$$

IV-lin-2d-strong (f_y linear in x , strong non-additive confounding)

$$\begin{aligned} f_x(z, c, e_x) &= 0.5z + 2c + e_x \\ f_y(x, c, e_y) &= x_1 + x_2 - 3(x_1 + x_2)(c_1 + c_2) + e_y \end{aligned}$$

IV-lin-2d-weak (f_y linear in x , weak non-additive confounding)

$$\begin{aligned} f_x(z, c, e_x) &= 2z + c + e_x \\ f_y(x, c, e_y) &= 5x_1 + 6x_2 - x_1(c_1 + c_2) + e_y \end{aligned}$$

IV-quad-2d-strong-add (f_y quadratic in x , strong additive confounding)

$$\begin{aligned} f_x(z, c, e_x) &= z + 2c + e_x \\ f_y(x, c, e_y) &= 2x_1^2 + 2x_2^2 - (c_1 + c_2) + e_y \end{aligned}$$

IV-quad-2d-weak (f_y quadratic in x , weak non-additive confounding)

$$2f_x(z, c, e_x) = 2z + c + e_x$$

$$f_y(x, c, e_y) = 5x_1^2 + 6x_2^2 - (x_1 + x_2)(c_1 + c_2) + e_y$$

3D treatment. The noises, confounders, and instruments follow

$$c, z, e_x \sim \mathcal{N}^3(0, 1)$$

$$e_y \sim \mathcal{N}(0, 1)$$

IV-quad-3d-weak (f_y quadratic in x , weak non-additive confounding)

$$f_x(z, c, e_x) = 2z + c + e_x$$

$$f_y(x, c, e_y) = 2x_1^2 + 2x_2^2 + 2x_3^2 - 0.3(x_2 + x_3)(c_1 + c_2 + c_3) + e_y$$

Leaky Mediator

We now describe datasets following the leaky mediator model with noises, and confounder following

$$e_x, e_m, c, u \sim \mathcal{N}^2(0, 1)$$

$$e_y \sim \mathcal{N}(0, 1)$$

LM-lin1-2d (f_y linear in x , strong confounding)

$$f_x(u, e_x) = u + e_x$$

$$f_m(x, c, e_m) = x + 3c - e_m$$

$$f_y(m, c, u, e_y) = 2m_1 + m_2 - (m_1 + m_2)(c_1 + c_2 + u_1 + u_2) + e_y$$

LM-lin2-2d (f_y linear in x , weak confounding)

$$f_x(u, e_x) = u + e_x$$

$$f_m(x, c, e_m) = 3x + c - e_m$$

$$f_y(m, c, u, e_y) = 2m_1 + m_2 - 0.3(m_1 + m_2)(c_1 + c_2 + u_1 + u_2) + e_y$$

D Response Functions

Our choice of response functions is characterized by the choice of K basis functions, as we saw in Equation (4). We primarily use the *neural basis functions* described in Section 4.3. Note that a linear combination of basis functions allows us to be arbitrarily expressive with our choice of family of response functions, and we can choose. In particular, we consider the following options:

1. *Neural basis functions:* The basis function ψ_k is the activation of the k th neuron in the last hidden layer of an MLP which has been trained on the observed data $\{(x_i, y_i)\}_{i \in [n]}$ to learn y given x .

In practice, we train a 3-hidden layer MLP with 64 neurons in the first two layers, rectified linear units

(ReLU) as activation functions and an MSE (mean squared error) loss for 100 epochs and a batch size of 512 using Adam with a learning rate of 0.01. The size K of the last hidden layer is equal to the number of basis functions we wish to have in our family of response functions.

An implicit assumption we have here is that the MLP can find a good approximation of y given x . This assumption is well supported by theoretical and empirical results showing the approximation power of neural networks (Shen et al., 2021; Daubechies et al., 2021), making it the perfect candidate for multi-dimensional treatments.

2. *Polynomials:* For a multivariate input $x = (x_1, x_2 \dots x_d)$, a response function can be considered to be a multivariate polynomial polynomial in x . However, in this case we would have 2^d different basis functions of degree up to d . This leads to the question of what basis functions to use here so as to have enough expressive power, but not blow up the number of basis functions and hence the dimension of the optimization parameter θ (see Equation (4)). Due to this blowup in the choice of basis functions with the dimension of the treatment in the case of polynomials, mainly use the neural basis functions.

In the cases when we do use the polynomial basis, we restrict ourselves to having upto quadratic terms in the basis function. For a d -dimensional treatment, this amounts to having a $d(d+3)/2 + 1$ dimensional θ .

3. *Gaussian process basis functions (GP):* We do not use this family of response functions, but mention them as a possible option. There is some previous work which considers the GP basis to define a family of functions (Kilbertus et al., 2020a). In this approach a Gaussian process is fit to K different sub-samples $\{(x_i, y_i)\}_{i \in N'}$ with $N' \leq N$. A single function is then sampled from each Gaussian process as the basis functions ψ_k for $k \in [K]$. Here, ‘sampling a function’ means to get the evaluation of the function at several points in the treatment space and then interpolate. While this is a reasonable approach when the treatment is scalar, for a multidimensional treatment, this requires the interpolating a multivariate function. The complexity and computational cost of such an interpolation increases with the increase in dimensionality, while the reliability of the interpolated function decreases at the same time. Also, higher dimension require exponentially higher number of point evaluations to get good interpolations. Due to these reasons, the GP basis approach is not found suitable for higher dimensions. However, it can be a viable options for scalar treatments.

E Implementation Details

We use $n = 10\,000$ data points for all our simulations. All implementation is in Python, using PyTorch (Paszke et al., 2019). Code for the experiments is provided with

the supplementary material.

E.1 Satisfying [c-data]

In Section 3.4 we explained how we match the observed data distribution by matching scalar statistics for L dictionary functions $\{\phi_l : \mathcal{Y} \rightarrow \mathbb{R}\}_{l=1}^L$. In practice, we take $L = 2$ and match the first and second moments of $Y | \{X, Z\}$, which is to say that we set $\phi_1(Y) = Y$ and $\phi_2(Y) = Y^2$. We learn ϕ_1 and ϕ_2 by regressing MLPs on the observed data $\{x_i, z_i, y_i\}_{i \in [n]}$ and $\{x_i, z_i, y_i^2\}_{i \in [n]}$ respectively, with $\{x_i, z_i\}_{i \in [n]}$ as the input and $\{y_i\}_{i \in [n]}$ and $\{y_i^2\}_{i \in [n]}$ as the target values. The outputs of these MLPs are then approximations of $\mathbb{E}[Y | X, Z]$ and $\mathbb{E}[Y^2 | X, Z]$, respectively. A significant advantage of this approach is that we can evaluate the constraints in closed form under our construction (see Equation (8)). We use MLPs with 3 hidden layers of sizes (64, 32, 16) (first to last) and train it with a batch size of 512 for 200 epochs, with a learning rate of 0.01. We use ReLU activations. Identical settings were used for the leaky mediator, with the only difference being that we match $Y | \{M, X\}$ instead of $Y | \{X, Z\}$.

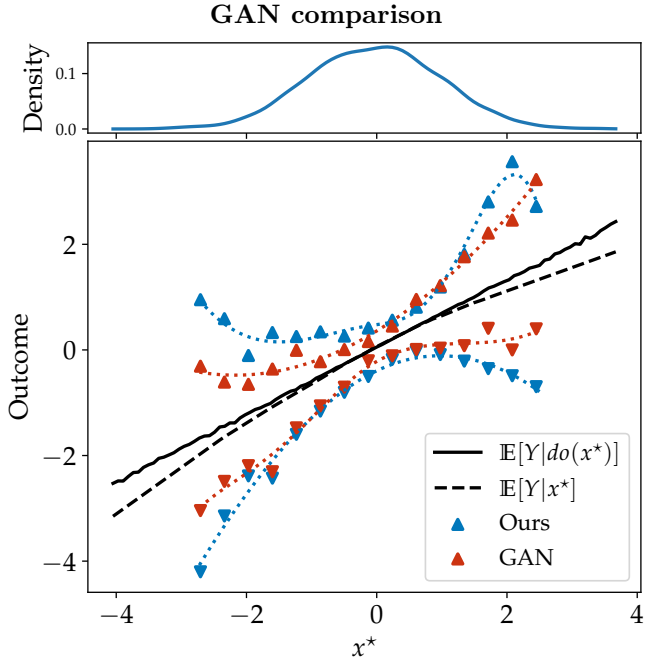


Figure 8: IV-lin-2d-weak.

E.2 Satisfying [c-struct]

We describe in Section 3.3 how we write the mean and variance of X as a function of Z . We considered two distinct ways of modeling $X | Z$.

Gaussian. We write the mean and variance of X as a function of Z . That is to say, $X = h_Z(N) := A(Z)N + b(Z)$. We parameterize $A(Z)$ as $A = L^\top L + \Omega$. A Cholesky factor $L : \mathcal{Z} \rightarrow \mathbb{R}^{p \times p}$ ensures symmetry and a diagonal matrix Ω adds small constants to the diagonal to ensure symmetry and positive definiteness. We then learn $L^\top L + \Omega$ from observed data \mathcal{D} by maximizing the log-likelihood of $\hat{p}(X | Z)$. In practice, the parameters

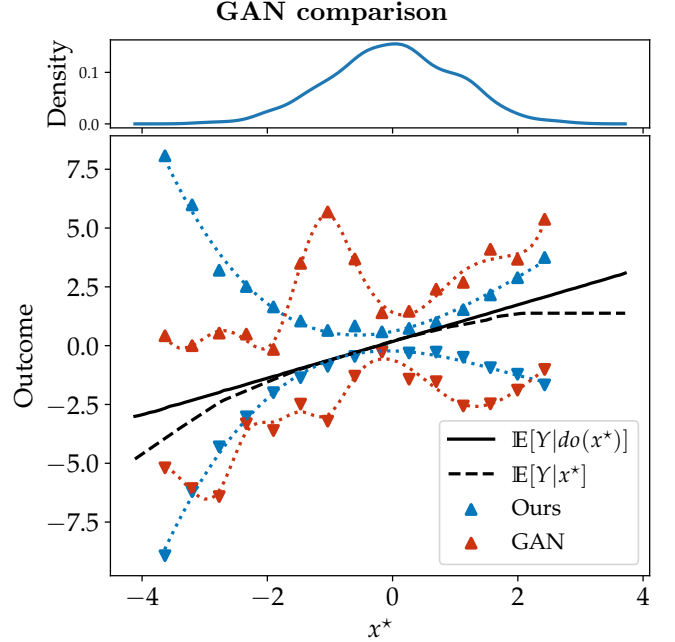


Figure 9: LM-lin-2d-weak.

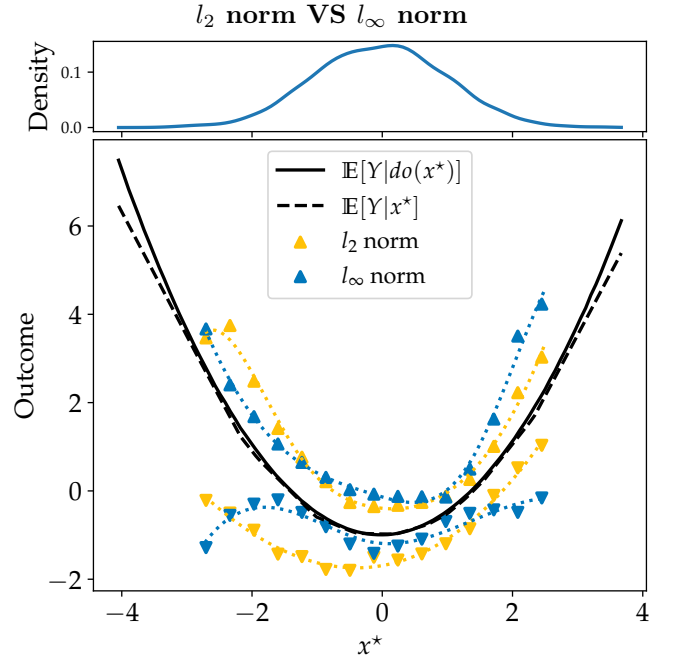


Figure 10: IV-quad-weak. Partially identifiable multi-dimension treatment. The l_2 norm includes all

of $A(Z)$ as described above, and the parameters of $b(Z)$ (which are just the entries of the vector $b(Z)$) are the output of an MLP which takes in Z . We learn the weights of this neural net once up front from observed data \mathcal{D} by maximizing the log-likelihood of $\hat{p}(X | Z)$. In practice, this MLP has 3 hidden layers of sizes (64, 32, 16) (first to last) and is trained with a batch size of 512 for 200 epochs, with a learning rate of 0.01. We use ReLU activations.

Conditional normalizing flow. We use an invertible (conditional) normalizing flow to model the distribution of $X | Z$. Flows are a natural candidate for modeling

distributions, and in this case follow both the properties we want from the modeling of $X | Z$. (i) Given X, Z , we can invert the transformation to get N . (ii) We can sample from $X | Z = z$. We use the Python library `pyro` [Bingham et al. \(2019\)](#).

All the experiments shown in this work use conditional normalizing flows due to better performance and stable optimization. However, the *Gaussian modeling* is described to point out one more way in which prior assumptions on functional dependencies could be incorporated in our generic framework. Once again, the construction is identical for the leaky mediator setting. The only difference is that there we model $M | X$ instead of $X | Z$.

E.3 Parameterizing \mathcal{S}

We consider θ to be K -dimensional and use the *neural basis function* in all experiments unless specified otherwise. Equation (5) describes how we parameterize our model. Here $\theta | N$ is parameterized by two MLPs with parameters with weights denoted by η_0 and η_1 . The weights of this MLP constitute our main optimization parameters η and we denote the outputs by μ_{η_0} and Σ_{η_1} . μ_{η_0} has 2 hidden layers with size (16, 16) and Σ_{η_1} has 2 hidden layers with size (32, 32). To evaluate the objective function, we perform Monte Carlo estimation $\mathbb{E}_N[\mu_{\eta_0}(N)]$ with 500 samples for N as in Equation (9).

The difference in the leaky mediator setting is that the parameterization of θ has 2 noise inputs instead of 1, as described in Appendix A. The remaining implementation choices remain unchanged.

E.4 Solving the optimization

The various MLPs described in the previous sections eventually lead to the formulation of a constrained optimization problem that we have seen in Equation (9).

We use the augmented Lagrangian method for inequality constraints to solve the constrained optimization problem in Equation (9). The formulation is taken from Section 17.3 in [\(Nocedal and Wright, 2006\)](#).

We have seen in Section 3.5 that we have a total of $N \cdot L$ constraints. We can think of $\hat{\phi}_l(x_i, y_i)$ as target values, estimated once up front from observed data. We denote $\hat{\phi}_l(x_i, y_i) = B_{l,i}$. The right-hand side $A_{l,i}$ is a function of the optimization parameter η as seen in Section 3.4. For ease of notation, we “flatten” the indices n and l into a single index $l \in [N \cdot L]$. We set the constraint slack to be the same value for each constraint, so $\epsilon_L = \epsilon$.

Then our set of constraints is

$$c_l(\eta) := \epsilon - |B_l - A_l(\eta)| \geq 0$$

With this, the Lagrangian we aim to minimize with respect to η can be formulated as:

$$\mathcal{L}(\eta, \lambda, \tau) := \pm o_{x^*}(\eta) + \sum_{l=1}^{N \cdot L} \xi(c_l(\eta), \lambda_l, \tau) \quad (14)$$

with

$$\xi(c_l(\eta), \lambda_l, \tau) := \begin{cases} -\lambda_l c_l(\eta) + \frac{\tau c_l(\eta)^2}{2} & \text{if } \tau c_l(\eta) \leq \lambda_l, \\ -\frac{\lambda_l^2}{2\tau} & \text{otherwise,} \end{cases}$$

where $-/+$ is used for the upper/lower bound. τ is increased throughout the optimization procedure and is seen as a temperature parameter. Given an approximate minimum η of this subproblem, we then update λ and τ according to $\lambda_l \leftarrow \max\{0, \lambda_l - \tau c_l(\eta)\}$ and $\tau \leftarrow \alpha \cdot \tau$ for all $l \in [N \cdot L]$ and a fixed $\alpha > 1$. The overall strategy is to iterate between minimizing Equation (14) and updating λ_l and τ . We find empirical justification in our experiments, where the approach reliably converges on a range of different datasets. We summarize our proposed procedure in Algorithm 1.

We have already seen how the basis function is chosen, how we can write the A of the constraints in closed form, how the B of the constraints is fixed upfront using ϕ_1 and ϕ_2 , and how the objective is estimated. It now remains, to solve this optimization problem, which we solve using the augmented lagrangian method as described in S. In practice we fix the initial value of τ to be $\tau_{init} = 10$, and the multiplier α to be 5, meaning that τ is updated by multiplying it by 1.08 at each step. The max value of τ is fixed at $\tau_{max} = 10,000$. We use 30 optimization steps to find the approximate optimal x_k at the k^{th} round of the optimization, and perform 150 round of optimization (number of times λ is updated) for each value of x^* and each bound (upper and lower). The optimization was performed using the Adam optimizer with a learning rate of 0.001. All of this again is through the use of auto-differentiation in PyTorch [Paszke et al. \(2019\)](#), implemented in python.

E.5 Hyperparameter search

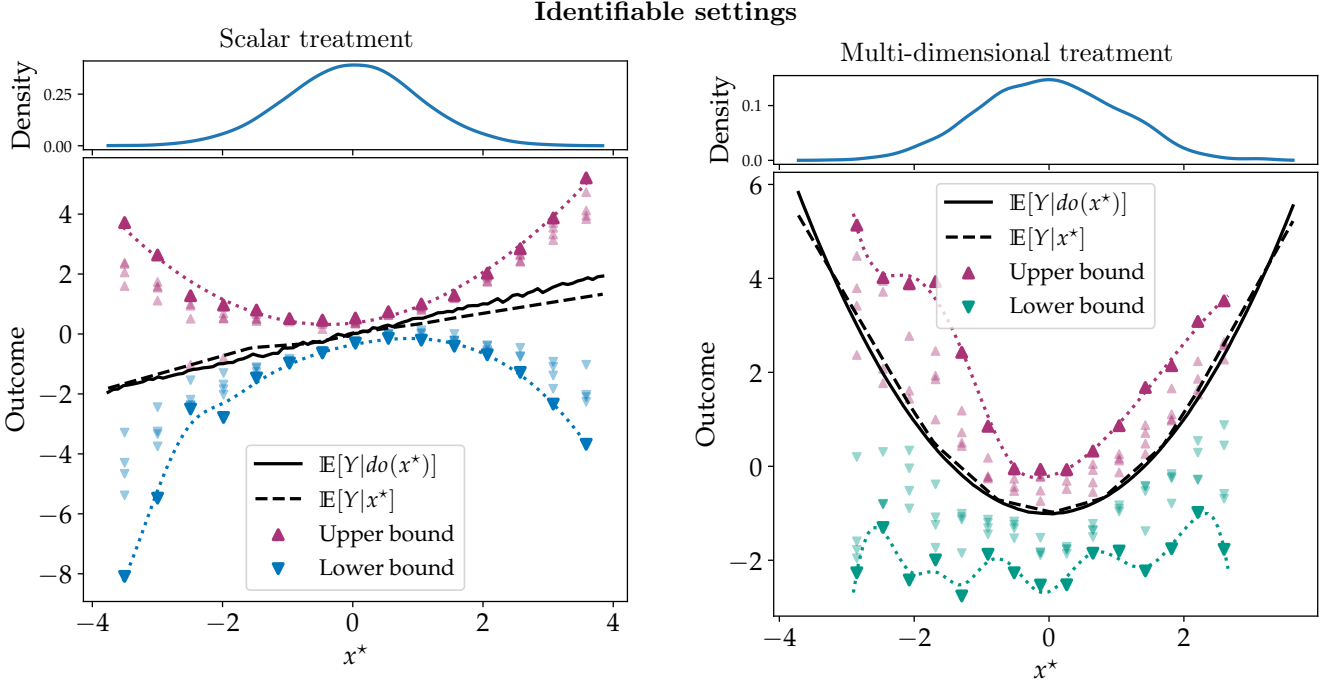
We did not perform an automated hyperparameter search for τ_{init} , τ_{max} and $\tau_{factor} = \alpha$ since we observed that the values $\tau_{init} = 10$, $\tau_{max} = 100000$ and $\tau_{factor} = 5$ worked reasonably well in all our settings. We arrived at this value through trial and error. An automated hyperparameter search can also be expected to improve the bounds.

E.6 Computational resources

We used a computing cluster provided by the university, for ease of parallelization of experiments. We used 1 CPU, 8000MB of RAM for all the x^* bounds for a single random seed for the method. To clarify, the use of the cluster was only for the purpose of running the optimization algorithm parallelly for various different random seeds. A single run of the algorithm (for getting bounds on multiple values of x^*) runs comfortably on a local machine with 16GB of RAM. No GPUs were used for the experiments.

F Further Experiments

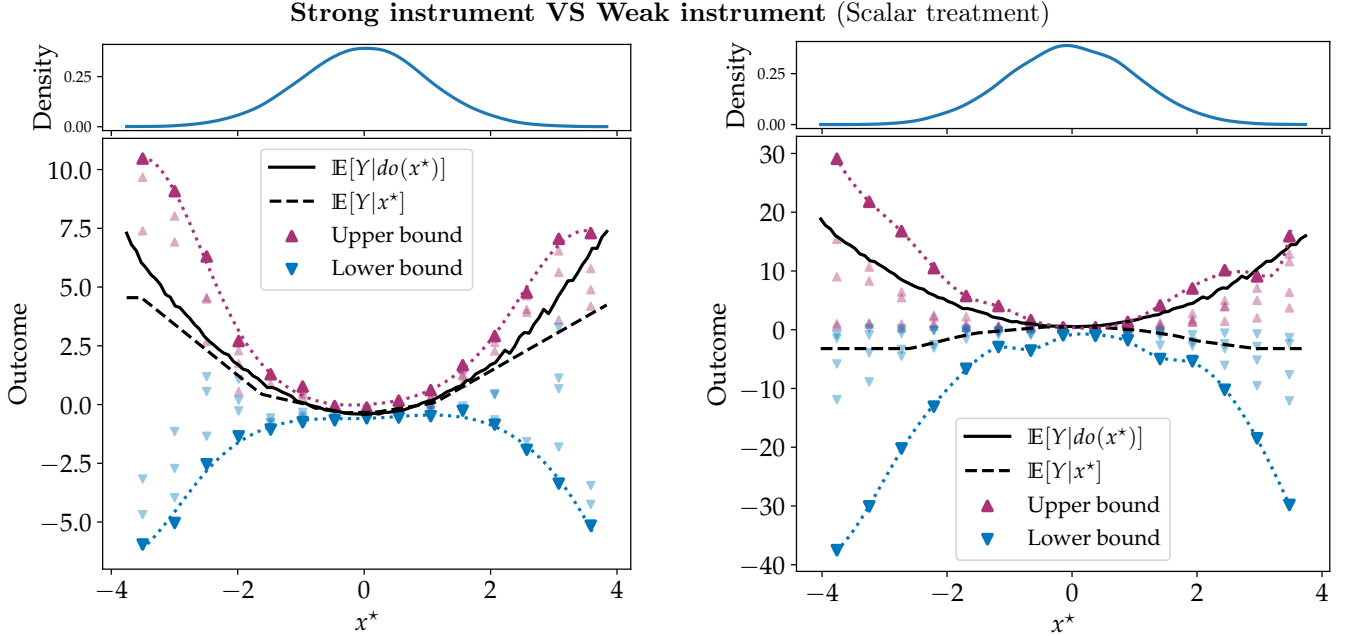
Here we show the performance of our method in a variety of settings.



(a) **IV-lin-1d-weak-add**. An identifiable scalar treatment with weak confounding. We get tight bounds despite using the neural basis functions.

(b) **IV-quad-2d-strong-add**. Multi-dimension treatment using the neural basis functions.

Figure 11: We see that our method is able to find tight bounds in identifiable settings in the data-dense regions.



(a) **iv-quad-1d-weak**. This is a partially identifiable scalar treatment setting. The bounds are particularly tight in the data-dense regions due to the strong instrument.

(b) **iv-quad-1d-strong**. This is a partially identifiable scalar treatment setting. The bounds are looser because the instrument is weak.

Figure 12: As expected, the bounds are tighter in the case of strong instrument.

F.1 Identifiable settings

Appendix E.3 shows the performance in the case of identifiable settings. We see that our method is able to find tight bounds in identifiable settings in the data dense regions. However, it is natural that the more expressive

the response function, the wider the bounds. This can potentially be used as a test of identifiability as described in Section 5. Such a test can be seen as a rather continuous measure of identifiability, giving an indication of being somewhere between identifiable and partially identifiable

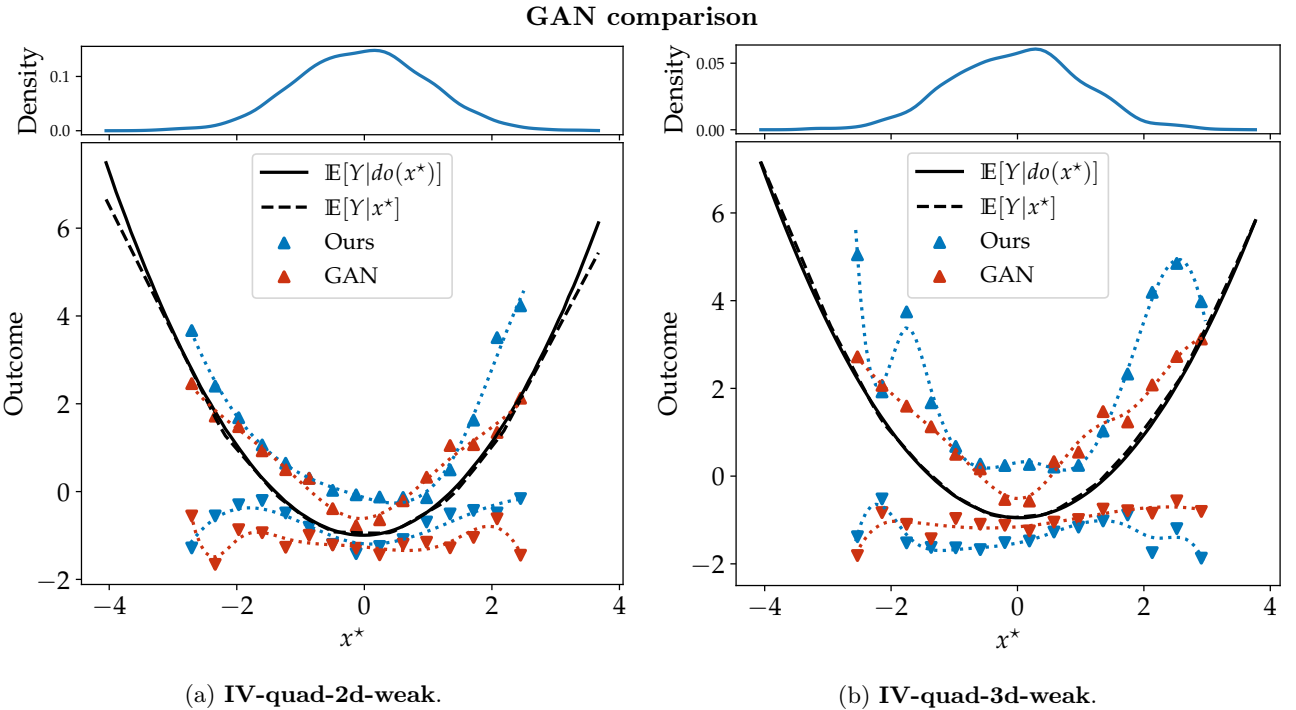


Figure 13: We do note that in this instance, the bounds given by our method are not as smooth in the data poor regions. However, our bounds are always valid, while the GAN framework gives some invalid bounds in both cases above.

based on the tightness of bounds, rather than being able to distinct strictly between identifiable and non-identifiable settings.

F.2 Strong instrument VS Weak instrument

Figure 12 compares the bounds in the cases of having a strong or weak instrument, or equivalently having weak or strong confounding relative to the instrument. As expected the bounds are looser when the confounding is stronger.

F.3 Comparing constraint norms

In Section 3.4 we have formulated our constraints in terms of norms. All the experiments so far have been using the $\|\cdot\|_{\infty, \infty}$ norm. Here we show experiments using the $\|\cdot\|_{2,2}$ norm as a constraint. This optimization procedure remains the same, but is potentially easier to solve since there is only 1 constraint now, but on the other hand this constraint is looser than matching the moment of each data point (or a chosen subsample). The results can be seen in Figure 10.

We point out that our formulation does not restrict us to norm based constraints. In fact given the generative model we have define in Section 3, we could also use any measure of distance between distributions as a constraint. However this would again lead to solving a bi-level optimization, making the optimization harder.

F.4 More comparisons to GAN bounds

We show some further comparisons of our method to the GAN bounds here. We see a similar trend where our bounds are generally smoother. The plots can be found in Figure 13, Figure 8 and Figure 9.

G Limitations of Kilbertus et al. (2020b)

Kilbertus et al. (2020b) limit the number of constraints by estimating $\mathbb{E}[\phi_l(Y) | z_i]$ only for a small pre-determined set of grid points z_i around which they bin the observed datapoints for empirical estimates. Thereby, they only constrain $p(Y | Z)$ instead of $p(Y | X, Z)$ and fundamentally limit themselves to low-dimensional settings, since otherwise the number of grid points grows exponentially with the dimension of Z . In particular, their proposed interpolation of empirical cumulative distribution functions to fix $p(x | z)$ in their copula model that parameterizes the distribution over θ virtually only allows one-dimensional instruments and treatments. Note that the binning procedure for Z also becomes problematic in the small data regime, where sufficiently many points are needed in each bin to keep the variance in the empirical mean and variance estimates low. As a consequence, the number of gridpoints in z must be carefully tuned depending on the dataset size.

Instead, our stochastic subsampling approach works with a fixed number of constraints for each update step inde-

pendent of the size of the dataset and the dimensionality of Z and X . In addition, we encode the structural assumptions into a graphical model for X, Z, θ that still allows for flexible conditional density estimation techniques such as invertible flows for individual components. The copula model had to rely on interpolated empirical cumulative density function estimated from potentially few datapoints within each bin. The Gaussian copula is also less flexible than our proposal. Finally, [Kilbertus et al. \(2020b\)](#) used Monte Carlo estimates both for the objective as well as for each individual constraint, often using different sample sizes for these estimates. Instead, we exploit the form of response functions as linear combinations of basis functions and compute the constraints in closed form, removing the additional variance from the stochastic optimization procedure. This leads to fewer tunable parameters and more robust convergence of the optimization.